Polymer Chemistry

Accepted Manuscript

This is an *Accepted Manuscript*, which has been through the Royal Society of Chemistry peer review process and has been accepted for publication.

Accepted Manuscripts are published online shortly after acceptance, before technical editing, formatting and proof reading. Using this free service, authors can make their results available to the community, in citable form, before we publish the edited article. We will replace this *Accepted Manuscript* with the edited and formatted *Advance Article* as soon as it is available.

You can find more information about *Accepted Manuscripts* in the Information for Authors.

Please note that technical editing may introduce minor changes to the text and/or graphics, which may alter content. The journal's standard Terms & Conditions and the Ethical guidelines still apply. In no event shall the Royal Society of Chemistry be held responsible for any errors or omissions in this *Accepted Manuscript* or any consequences arising from the use of any information it contains.

ROYAL SOCIETY OF CHEMISTRY

www.rsc.org/polymers

α-Tocopheryl succinate-based amphiphilic block copolymers obtained by RAFT and their nanoparticles for the treatment of cancer

Raquel Palao-Suay[1,2], María Rosa Aguilar[1,2], Francisco J. Parra-Ruiz[1], Samarendra Maji[3], Richard Hoogenboom[3], N.A.Rohner[4], Susan N. Thomas[4] and Julio San Román[1,2]*

[1]Group of Biomaterials, Department of Polymeric Nanomaterials and Biomaterials, Institute of Polymer Science and Technology, CSIC, Juan de la Cierva, 3, 28006 Madrid, Spain

[2]Networking Biomedical Research Centre in Bioengineering, Biomaterials and Nanomedicine, CIBER-BBN, Spain

[3]Supramolecular Chemistry Group. Department of Organic and Macromolecular Chemistry. Ghent University. Krijgslaan 281-S4, 9000 Ghent, Belgium

[4]George W. Woodruff School of Mechanical Engineering and Parker H. Petit Institute of Bioengineering and Bioscience, Georgia Institute of Technology, 315 Ferst Dr NW, Atlanta, 30332 Georgia, USA

Corresponding author (*): Dra. María Rosa Aguilar

Email: mraguilar@ictp.csic.es

Telephone: +34 91561 88 06 (ext.212)

Fax: +34 91 564 48 53

KEYWORDS: α-tocopheryl succinate, poly(ethylene glycol), RAFT polymerization, self-organized precipitation, self-assembled nanoparticle.

ABSTRACT

α-Tocopheryl succinate (α-TOS) is a well-known mitochondrially targeted anticancer compound. However, the major factor limiting the use of α-TOS is its low solubility in physiological media. To overcome this problem, the aim of this work is the preparation of new polymeric and active α-TOS-based nanovehicle with a precise control over its macromolecular architecture. Reversible addition-fragmentation chain transfer polymerization (RAFT) is used to synthesize an α-TOS amphiphilic block copolymer with highly homogeneous molecular weight and relatively narrow dispersity. Macro-chain transfer agents (macro-CTA) based on poly(ethylene glycol) (PEG) of different molecular weights (MW, ranging from 4.6 to 20 kDa) are used to obtain block copolymers with different hydrophilic/hydrophobic ratios with PEG being the hydrophilic block and a methacrylic derivative of α-tocopheryl succinate (MTOS) being the monomer that formed the hydrophobic block. PEG-*b*-poly(MTOS) form spherical nanoparticles (NPs) by self-organized precipitation (SORP) or solvent exchange in aqueous media enabling to encapsulate and deliver hydrophobic molecules in their core. The resulting NPs are rapidly endocytosed by cancer cells. The biological activity of the synthesized NPs are found to depend on the MW of PEG, with NP comprised of the higher MW copolymer resulting in the lower bioactivity due to PEG shielding inhibiting cellular uptake by endocytosis. Moreover, the biological activity also depends on the MTOS content, as the biological activity increases as a function of MTOS concentration.

INTRODUCTION

The rapid growth of nanomedicine has opened the possibility to create sophisticated strategies against cancer and other diseases at a nanoscale where the properties of materials often differ from those of the corresponding bulk materials[1, 2]. As such, a wide range of materials based on natural or synthetic polymers are available to design self-assembled nanostructures[3-5]. Macromolecular self-assembly represents a spontaneous process that involves the organization of amphiphilic macromolecules in an aqueous environment, forming different supramolecular structures[6, 7]. One interesting example of this variety of supramolecular assemblies is nanoparticles (NPs) that exhibit a core-shell morphology based on the use of amphiphilic polymers with hydrophobic and hydrophilic domains[8-10].

The preparation of advanced nano-assemblies using amphiphilic copolymeric systems requires the optimal control over the chemical composition and distribution of monomeric units into the macromolecular chains. In this sense, amphiphilic polymers can be obtained by different synthetic methodologies, such as free radical or controlled radical polymerization (CRP). Both techniques proceed via the analogous radical mechanism. However, conventional free radical polymerization does not allow the complete control of the molecular weight (MW) and therefore, heterogeneous mixtures of macromolecular chains are obtained. Thus, CRP methods have emerged as potent tools for the synthesis of macromolecular architectures that exhibit a narrow dispersity and controlled MW[11]. Among them, Reversible Addition-Fragmentation Chain Transfer (RAFT) polymerization is one of the most versatile polymerization technique because it can be applied with a great variety of functional monomers using mild reactions conditions and avoiding the use of metal catalysts [12, 13].

α-Tocopheryl succinate (α-TOS) is a well-known vitamin E derivative that has been described as a mitochondrially targeted anticancer compound (mitocan) with anticancer and anti-angiogenic properties[14-16]. In fact, this molecule selectively induces apoptosis of cancer and proliferating cells by the displacement of ubiquinone by binding to complex II and by the disablement of Bcl-2 or Bcl-xL anti-apoptotic proteins in the mitochondria electron transport chain[17-19]. The combination of these complementary actions produces high levels of reactive oxygen species (ROS) that activates the intrinsic apoptosis cascade and therefore induces cell death after exposure[20].

Despite the potential and attractive activity of α-TOS, its hydrophobic nature significantly limits its successful use in cancer therapy as it causes high toxicity and reduced bioavailability. For that reason, the development of α-TOS based delivery systems is desirable[21]. Specifically, one strategy to increase the bioavailability and stability of α-TOS has been the conjugation of poly(ethylene glycol) (PEG), obtaining PEG_{1000}-α-TOS conjugate (TPGS)[22, 23]. In fact, this macromolecule has been approved by the FDA as an adjuvant at concentrations lower than 0.02 wt %, and it presents an emulsification effect 67 times higher than other surfactants such as PVA[24]. For that reason, this molecule has been incorporated in the formulation of biodegradable nanoparticles based on poly(lactic-*co*-glycolic acid) (PLGA)[25-27], polylactic acid (PLA)[28-30] and poly(ε-*caprolactone*) (PCL)[31, 32]. In spite of enhancements in solubility, permeability and stability, TPGS-based nano-assemblies have important disadvantages for their use as anti-cancer agents. Particularly, these nanoparticles exhibit cytotoxicity against healthy cells without optimal selectivity toward tumour tissues or cancerous cells. Additionally, TPGS-based nano-formulations incorporate a limited amount of α-TOS into the macromolecular system and the MW of PEG chains is not enough to avoid

the opsonization by the reticuloendothelial system (RES)[33]. These limitations could be surmounted, however, through the development of an effective α-TOS delivery system.

Our group has extensively experience in the preparation of drug delivery systems of hydrophobic drugs[34-37]. In fact, we recently described the preparation of amphiphilic copolymers of *N*-vinyl pyrrolidone (VP) and a methacrylate derivative of α-TOS (MTOS) by free radical polymerization [38]. However, the development of self-assembling systems based on α-TOS with precise control over the macromolecular architecture has not been achieved. For that reason, the goal of this work was the preparation of new amphiphilic nano-assemblies as drug delivery systems of α-TOS using PEG as a hydrophilic domain, PMTOS as hydrophobic block, and using RAFT as a polymerization method enabling the preparation of defined block copolymers (**figure 1**).

The selection of PEG as hydrophilic macromolecule was based on its biocompatibility and non-toxicity and its capacity to create a hydrophilic shell that can improve the accumulation of NPs into the tumor tissues by the enhanced permeation and retention effect. This effect is only feasible with the use of an appropriate MW of PEG, higher than 3 kDa, that enhance the stealth character of NPs, avoiding the RES system[33, 39]. In this sense, the effect of PEG block length was studied by the preparation of PEG based chain transfer agents (PEG macro-CTA agents) with different MW (between 4.6 and 20 kDa). The RAFT polymerization of MTOS with these different PEG macro-CTA agents allowed the incorporation of a controlled number units of its active drug into the macromolecular chains. The formation of self-assembled nanoparticles by self-organized precipitation (SORP) was also investigated with the complete characterization of their physico-chemical properties. The anticancer activity of MTOS based NPs were examined against breast cancer cells (**figure 1**).

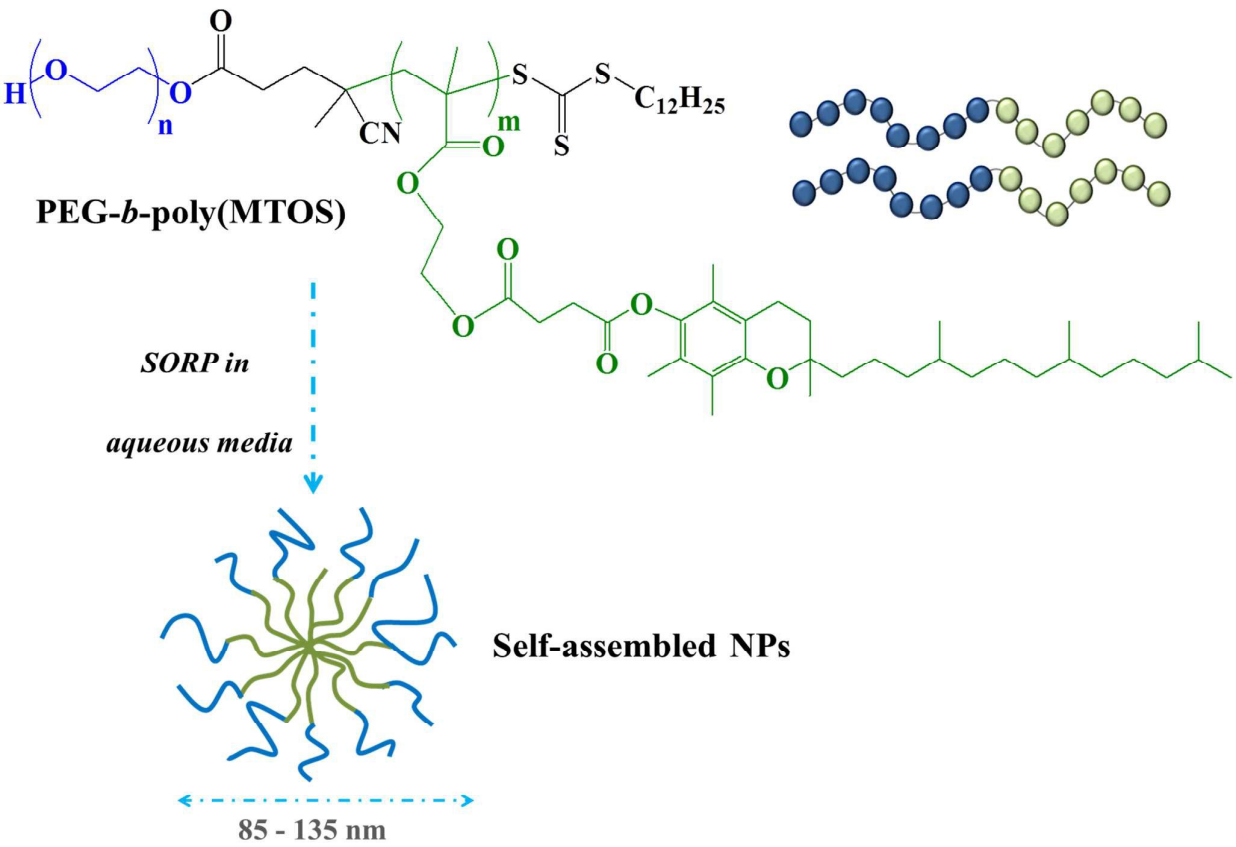

Figure 1: Chemical structure of PEG-*b*-poly(MTOS). Scheme of the self-assembled NPs formation based on these block copolymers, prepared by SORP or solvent exchange.

MATERIALS AND METHODS

Materials

Poly(ethylene glycol) (PEG, number average MW (M_n) between 4.6 and 20 kDa, Sigma-Aldrich), 4-cyano-4-[(dodecylsulfanylthiocarbonyl)sulfanyl]pentanoic acid (CTA, Sigma-Aldrich), *N*-(3-dimethylaminopropyl)-*N'*-ethylcarbodiimide hydrochloride (EDC, Sigma-Aldrich), 4-dimethylaminopyridine (DMAP, Sigma-Aldrich), $MgSO_4$ anhydrous (Qemical), dichloromethane (CH_2Cl_2, Sigma-Aldrich), hexane (SDS) and diethylether (SDS) were used without further purification in the preparation of different macro-chain transfer agent (CTA). 2,2'-Azobisisobutyronitrile (AIBN, Merck) was recrystallized from methanol (m.p. 104 ºC) before use. Deuterated chloroform ($CDCl_3$, Sigma-Aldrich) and chromatographic grade tetrahydrofuran (THF, Sigma-Aldrich) were used without further purification to characterize polymeric systems. Additionally, sodium chloride (NaCl, Panreac) and coumarin-6 (c6, Sigma-Aldrich) were used without further purification.

Characterization techniques

^{1}H-NMR and ^{13}C-NMR spectroscopy were performed in a Mercury 400BB apparatus, operating at 400 and 100 MHz, respectively. The spectra were recorded by dissolving the corresponding sample in $CDCl_3$ at 25 ºC. Fourier transform infrared attenuated total reflectance (FTIR-ATR) spectroscopy was obtained in a Perkin Elmer Spectrum One FTIR spectrometer using 32 scans, and a resolution of 4 cm^{-1}.Thermogravimetric analysis were performed using a TGA Q500 apparatus (TA instruments), under dynamic nitrogen atmosphere at a heating rate of 10 ºC/min in a range of 25–600 ºC with the aim to study the thermal stability of the polymeric systems. The number and weight average molecular weight (M_n and M_w) and dispersity (Đ) of all the polymers

were determined by size exclusion chromatography (SEC) using a Perkin-Elmer Isocratic LC pump 250 coupled to a refraction index detector (Series 200). Three polystyrene-divinyl benzene columns (PLgel, Varian, Polymer Laboratories) of average pore size of 10^3, 10^4 and 10^5 Å were used as solid phase, and degassed THF (1 mL/min) was used as eluent at 40ºC. Monodisperse poly(methyl methacrylate) (PMMA) standards (Scharlab) with MW between 10.3 and 1,400 kDa were used to obtain the calibration curve. Data were analyzed using the Perkin-Elmer LC solution program.

Preparation of block copolymers by RAFT polymerization

Synthesis of the methacrylic derivative of the α-tocopheryl succinate (MTOS)

MTOS was obtained as previously described[38]. *N,N'*-dicyclohexylcarbodiimide (DCC,1.5 equivalent) in CH_2Cl_2 was added dropwise to a solution of α-tocopherol (α-TOH, 1 equivalent), mono-(2-(methacryloyloxy)ethyl) succinate (MES, 1.4 equivalent) and DMAP (0.1 equivalent) in CH_2Cl_2. The reaction was stirred for 24 h under nitrogen atmosphere at room temperature. The reaction mixture was washed with NaOH (1N) and HCl (1N), dried over $MgSO_4$ and the solvent was removed under reduced pressure.

Synthesis of PEG macro-CTA agents

The modification of the commercial 4-cyano-4-[(dodecylsulfanylthiocarbonyl)sulfanyl]pentanoic acid CTA was performed by EDC coupling in order to incorporate PEG of different MW between 4,6 and 20 kDa. For this purpose, diverse PEG (1 eq) and CTA (1.2 eq) were dissolved in CH_2Cl_2 and introduced into a 250 mL round-bottom flask. Additionally, EDC (1.5 eq) and DMAP (0.12 eq) in CH_2Cl_2 were then added drop wise with constant stirring using an ice bath under nitrogen atmosphere. Afterwards, the reaction mixture was stirred for 24 h at room temperature.

The reaction mixture was washed with milliQ water and the solvent was removed under reduced pressure. The resulting product was resolved in the minimal volume of CH_2Cl_2 and precipitated in a cold mixture of hexane and diethylether (50:50 v:v). After drying over $MgSO_4$, the residual solvent was removed under reduced pressure until constant weight. The yield of the reaction was 90%. The chemical structure of the different PEG macro-CTA agents was elucidated by NMR spectroscopy.

^{1}H-NMR spectrum (400 MHz, $CDCl_3$): δ_H 4.25 (t, J = 4.8 Hz, 2H), 3.72 (t, J = 4.8 Hz, 2H), 3.64 (s, 749H), 3.32 (t, J = 7.5 Hz, 2H), 2.65 (m, 2H), 2.52 (m, 1H), 2.37 (m, 1H), 1.87 (s, 3H), 1.68 (quint, J = 7 Hz, 2H), 1.39 ((quint, J = 7.6 Hz, 2H), 1.33-1.21 (m, 16H), 0.87 (t, J = 7 Hz, 3H) ppm.

^{13}C-NMR spectrum (100 MHz, $CDCl_3$): δ_C 171.6, 119.2, 77.5, 72.7, 71.9, 70.7, 70.5, 70.3, 69.6, 69.1, 46.5, 37.2, 34.0, 32.1, 29.9, 29.8, 29.7, 29.6, 29.2, 29.1, 27.9, 25.0, 22.9, 14.3 ppm.

ATR-FTIR spectrum (cm^{-1}): υ = 2950, 2884, 2803, 2744, 2695, 2167, 1973, 1740, 1467, 1414, 1360, 1342, 1279, 1242, 1146, 1101, 1060, 961, 952, 842 cm^{-1}.

RAFT polymerization

Block copolymers based on MTOS and different PEG-macro CTA agents were synthesized by RAFT polymerization. Particularly, PEG-macro CTA agent, MTOS, AIBN and anhydrous 1,4-dioxane were sealed in a 25 mL Schlenk tube. The reaction mixture was degassed by three freeze-pump-thaw cycles and heated in an oil bath at 70 ^{o}C under magnetic stirring. The total monomer concentration [M], the reaction time and the feed molar ratio [MTOS]:[CTA]:[AIBN] were varied as a function of the PEG-macro CTA used for the copolymerization of MTOS (**table S1**). For the kinetic investigations, samples (250 µL) were taken from the polymerization mixture after different reaction times (30, 60, 90, 120, 180, 300 and 360 min). These samples were cooled and characterized using SEC and ^{1}H-NMR spectroscopy.

When the reaction time had elapsed, block copolymers were purified by dialysis (Spectrum Laboratories, 25 kDa MW cut-off) against a mixture of THF and water (50:50 v:v) that was gradually replaced by distilled water over three days in order to remove the residual unreacted monomers and low molecular weight species. The resulting solutions were isolated by freeze-drying to yield white amorphous powders. The conversion and chemical structure of block copolymers were elucidated by NMR spectroscopy using MestreNova 9.0 software.

^{1}H-NMR spectrum (400 MHz, $CDCl_3$): δ_H 4.46-3.88 (2xbs, 4H), 3.64 (s, 753 H) 2.89 (bs, 2H), 2.83-2.63 (bs, 2H), 2.54 (bs, sH), 2.10-1.90(3xs, 9H), 1.84-1.62 (m, 3H), 1.62-0.97 (m, 23H), 0.95-0.78 ppm (m, 12H).

^{13}C-NMR spectrum (100 MHz, $CDCl_3$): δ_C 172.1, 171.2, 171.1, 149.6, 140.7, 136.1, 126.9, 126.3, 125.2, 123.2, 123.1, 117.6, 117.5, 77.5, 75.2, 70.8, 62.5, 45.1, 39.6, 37.6, 37.5, 33.0, 32.9, 31.3, 29.0, 28.2, 25.0, 24.7, 23.0, 22.9, 21.3, 20.8, 20.0, 19.9, 13.1, 12.3, 12.0 ppm.

ATR-FTIR spectrum (cm^{-1}): υ = 2954, 2927, 2899, 2871, 1737, 1666, 1581, 1521, 1461, 1411, 1379, 1364, 1344, 1313, 1280, 1247, 1203, 1145, 1109, 1062, 996, 964, 944, 922, 863, 845, 818, 749, 681 cm^{-1}.

NPs formation by SORP

Surfactant-free NPs were prepared by SORP[40] or solvent exchange. Specifically, block copolymers were dissolved in 1,4-dioxane at 10 mg/mL. Additionally, an aqueous solution of NaCl (100 mM) was incorporated drop by drop over the organic phase under constant magnetic stirring to obtain a final polymer concentration of 5 mg/mL. c6 (1% w/w respect to the polymer) was also added to the organic phase in order to prepare NPs that entrapped this hydrophobic molecule in their inner core. After the precipitation, milky NP dispersions were dialyzed against NaCl during 72 h in order to remove organic solvent and unloaded c6. Afterwards, each NP suspension was sterilized by

filtration through 0.22 μM polyethersulfone membranes (PES, Millipore Express®, Millex GP) and stored at 4 ºC.

The encapsulation efficiency (EE) of c6 was measured by fluorescence spectroscopy. For this purpose, NPs were freeze dried and dissolved in ethanol (2 mg/mL) and their fluorescence was measured ($\lambda_{excitation}$ = 485 nm and $\lambda_{emission}$ = 528 nm) using a Biotek SYNERGY-HT plate reader. The fluorescence intensity was correlated with c6 concentration using a calibration curve at c6 concentrations between 0.5 – 0.001 mg/mL in ethanol.

Morphology, particle size Distribution and Zeta Potential

The morphology of NPs was analyzed by scanning electron microscopy (SEM) using a Hitachi SU8000 TED, cold-emission FE-SEM microscope working with an accelerating voltage between 25 and 50 kV. Samples were prepared by deposition of one drop of the corresponding NP suspension (0.05 mg/mL) over small glass disks. The aqueous phase was evaporated at room temperature for 24 h. The samples were coated with gold palladium alloy (80:20) prior to examination by SEM.

For AFM examination, a drop of NPs dispersion was deposited on a surface of small glass disks and dried overnight at room temperature. AFM was performed in tapping mode using a Multimode AFM (Veeco Instruments, Santa Barbara, CA, USA) with a Nanoscope IVa control system (software version 6.14r1), equipped with silicon tapping probes (RTESP, Veeco) with a spring constant of 42 N/m and a resonance frequency of 300 KHz and a scan rate of 0.5 Hz.

The particle size distribution of the self-assembled NPs was determined by dynamic light scattering (DLS) using a Malvern Nanosizer NanoZS Instrument equipped with a

4mW He-Ne laser (λ=633 nm) at a scattering angle of 173°. Measurements of NP dispersions were performed in square polystyrene cuvettes (SARSTEDT) at 25 ºC. The autocorrelation function was converted in an intensity particle size distribution with ZetaSizer Software 7.10 version, to get the mean hydrodynamic diameter (D_h, by intensity) and the polydispersity index (PDI) between 0 (monodisperse particles) and 1 (polydisperse particles) based on the Stokes-Einstein equation. The zeta potential was determined for NP formulations at 0.2 mg/mL concentration containing 10 mM NaCl and using laser Dopper electrophoresis (LDE). The zeta potentials were automatically calculated from the electrophoretic mobility using the Smoluchowski´s approximation. For each sample, the statistical average and standard deviation of data were calculated from 8 measurements of 20 runs each one.

Biological experiments

Cell culture

Human metastatic carcinoma cells, MDA-MB-453 cells (ATCC), were cultured in Dulbecco's modified Eagle's medium (DMEM), supplemented with 10% fetal bovine serum (FBS), 1% penicillin/streptomycin (PS) and incubated at 37°C and 5% CO_2.

Cellular uptake study: monitorization of coumarin-6 loaded NP

MDA-MB-453 cells were seeded into 6-well plate at 200,000 cells/mL in complete medium and incubated at 37 ºC for 48 h. Afterwards, the monolayer was washed with culture medium and subsequently incubated with the corresponding c6 entrapped NPs dispersed in NaCl (1000 µL of the NP suspension and 1000 µL of completed medium) at 37 ºC. At different time points (30 min, 1, 2, 4, 6 and 8 h) , NPs were removed and cells were washed four times with PBS in order to efficiently remove non-endocytosed

NPs by cells. Then, the cells were trypsinized (0.5 mL of Trysin-EDTA per well), centrifuged (10 min, 1500 rpm) and lysed with 0.4 mL of ethanol at room temperature. The c6 concentration in the cell lysate was quantified by fluorescence plate reader ($\lambda_{excitation}$ = 458 nm and $\lambda_{emission}$ = 540 nm). The cellular uptake was normalized to the total amount of cells for each sample.

The endocytosis of NPs was also visualized using a fluorescent EVOS® FL microscopy at the different experimental points. Particularly, the cells were fixed by a paraformaldehyde solution in PBS (3.7 w/v %) for 15 min at room temperature. In the same manner, cells were observed by Confocal Laser Scanning Microscopy (CLSM, LSM 710, Zeiss) after 4 h of NP treatment.

In vitro cytotoxicity assay

Cell viability in the presence of different concentrations of NPs (2.5, 1.25, 0.63, 0.31 and 0.16 mg/mL) was measured using Alamar Blue assay (Sigma-Aldrich) [41]. Briefly, MDA-MB-453 cells were seeded at 35,000 cells/mL (20,500 cells/well) in 24-well plates. After 24 h of incubation, the medium was replaced with the corresponding NPs dispersed in NaCl (50:50 v/v of the NP suspension and completed medium). The plates were incubated at 37°C in a humidified air with 5% CO_2 for 24 h. Afterwards, 100 µL of Alamar Blue solution (10 % Alamar Blue solution in phenol red free DMEM medium) was added to all wells. After 4 h of incubation, the fluorescence was measured on a Biotek SYNERGY-HT plate reader ($\lambda_{excitation}$ = 530 nm and $\lambda_{emission}$ = 590 nm).

Statistical analysis

Results were expressed as mean ± standard deviation. Statistical significance (significance level of: *: $p < 0.05$) was evaluated using the analysis of variance (ANOVA, Tukey test) as required, by Origin 9.

RESULTS AND DISCUSSION

PEG macro-CTA agents

RAFT polymerization is one of the most attractive and effective technique to synthesize well-defined polymers and therefore to prepare amphiphilic block copolymers with a precise control of their macromolecular nature[13]. This type of radical polymerization involves a chain transfer agent (CTA) that is commonly formed by a thiocarbonylthio moiety in order to exhaustively control the uniform chain growth, the generated MW of macromolecular chains and their dispersity. In fact, the selection of the most appropriate chain transfer agent is the key to reach an excellent control during the polymerization[12, 13, 42]. In particular, 4-cyano-4-[(dodecylsulfanylthiocarbonyl)sulfanyl]pentanoic acid was selected for the polymerization of MTOS due to the presence of a carboxylic end group that facilitates the conjugation of PEG to obtain a hydrophilic macro-CTA agent and its suitability to control the polymerization of methacrylic monomers[43].

PEG was selected as hydrophilic block because it is a water soluble, hydrophilic and biocompatible polymer that can reduce the adhesion of opsonins, avoiding the NP recognition by the RES and increasing the blood circulation half-life of polymeric NPs. Furthermore, PEG can be easily functionalized with different ligands for targeted drug delivery[44, 45]. Five different PEG macro-CTA agents were successfully synthesized in mild conditions by EDC coupling of PEG to the CTA, obtaining pure products after their purification. In fact, the synthesis of similar PEG based macro-CTA agents were previously reported in the literature[46, 47]. Particularly, EDC is one of the most widely used coupling agents to conjugate a carboxylic acid to an alcohol, using DMAP as a catalyst. Specifically, the esterification involves the activation of carboxylic acid by

EDC which forms an O-acylisourea intermediate. The most important advantage of EDC over other coupling agents like DCC is that the urea sub-product is readily soluble in water and can easily be removed by extraction, facilitating the purification of the final product[48-50].

The MW of PEG was varied between 4.6 and 20 kDa in order to change the length of this hydrophilic block and to analyse its influence in the physico-chemical properties of the polymeric systems and to change the hydrophilic/hydrophobic balance of the block copolymers. The MW of the PEG blocks were lower than 30 kDa, and therefore they can be cleared from the body through renal filtration[51]. Moreover, the MW is a critical factor to control the stealth properties of self-assembled systems, as will be described in the next sections. In this sense, the capacity to create a high-density of PEG chains on the surface of the NPs is diminished when its MW is lower than 3 kDa.

The esterification of the commercial RAFT agent was confirmed using ^{1}H-NMR spectroscopy by the appearance of the methylene protons of the PEG chains (CH_2-a at 4.2 ppm and CH_2-b-d between 3.35 and 3.85 ppm) (**figure S1, see Supporting Information**). The synthesized PEG macro-CTA agents were labelled as CTA-PEG and their MW (kDa) was determined by ^{1}H-NMR spectroscopy.

Results of number average MW (M_n), dispersity (Đ***)*** and the number of PEG units (nPEG) are summarized in the **table S2**. nPEG was quantitatively calculated by ^{1}H-NMR spectra by considering the signals between 3.30-3.85 ppm assigned to 4 protons of PEG backbone chains (CH_2-a, CH_2-b) and the signal at 0.81 ppm which is due to 3 protons of CTA (CH_3-19). In all PEG macro-CTA agents, Đ values were less than 1.20 and SEC traces evidenced that the esterification allowed to obtain monomodal and narrow MW distributions of the hydrophilic macro-CTA agents. All traces were shifted

to lower elution times in comparison to the commercial PEG after their esterification. Additionally, SEC traces of different PEG macro-CTA agents showed tailing peaks at lower molecular weight areas that are attributed to the original PEG (**figure S2**, see Supporting Information).

Thermal degradation curves of different PEG macro-CTA agents showed a single weight loss step at temperatures ranging from 320 and 440 ºC. The thermal decomposition rate presented a maximum around 400ºC that slightly increased with the MW of PEG block (**figure S3**, see Supporting Information).

Synthesis of block copolymers PEG-b-poly(MTOS)

The RAFT polymerization of MTOS was successfully performed with the synthesized PEG macro-CTA agents and AIBN as radical initiator, using the conditions that were previously summarized in the **table S1**. All copolymerizations were performed at 70ºC in anhydrous dioxane. Total molar concentration (M), ratio [MTOS]:[CTA]:[AIBN], and copolymerization time were optimized in order to control the polymerization reaction and avoid undesired termination reactions during the chain growth[52].

In order to prevent the gelation of the reaction product due to significant increase of the reaction medium viscosity, total MTOS concentration was reduced as the MW of the PEG macro-CTA increased (0.5 M for CTA-PEG_5, CTA-PEG_8, CTA-PEG_{10} and 0.25 M for CTA-PEG_{12} and CTA-PEG_{22}). Additionally, the concentration of AIBN was increased for the polymerizations of the highest PEG MW (CTA-PEG_{12} and CTA-PEG_{22}) in order to counteract the effect of the reduction of the total MTOS concentration, avoiding prolonged reaction times. Finally, the copolymerizations were stopped at the reaction time that allowed to maintain a linear kinetic of the reaction with an optimal Đ, as will be demonstrated in the following sections.

Polymerization of the MTOS was confirmed using ^{1}H-NMR spectroscopy by the disappearance of the vinyl protons of MTOS between 5.5 and 6.5 ppm and the broadening of the signals as a result of the macromolecular nature of the synthesized block polymers (**figure 2**). Additionally, other characteristics proton signals of MTOS could be appropriately assigned, confirming the presence of its chemical structure in the backbone of the copolymeric systems.

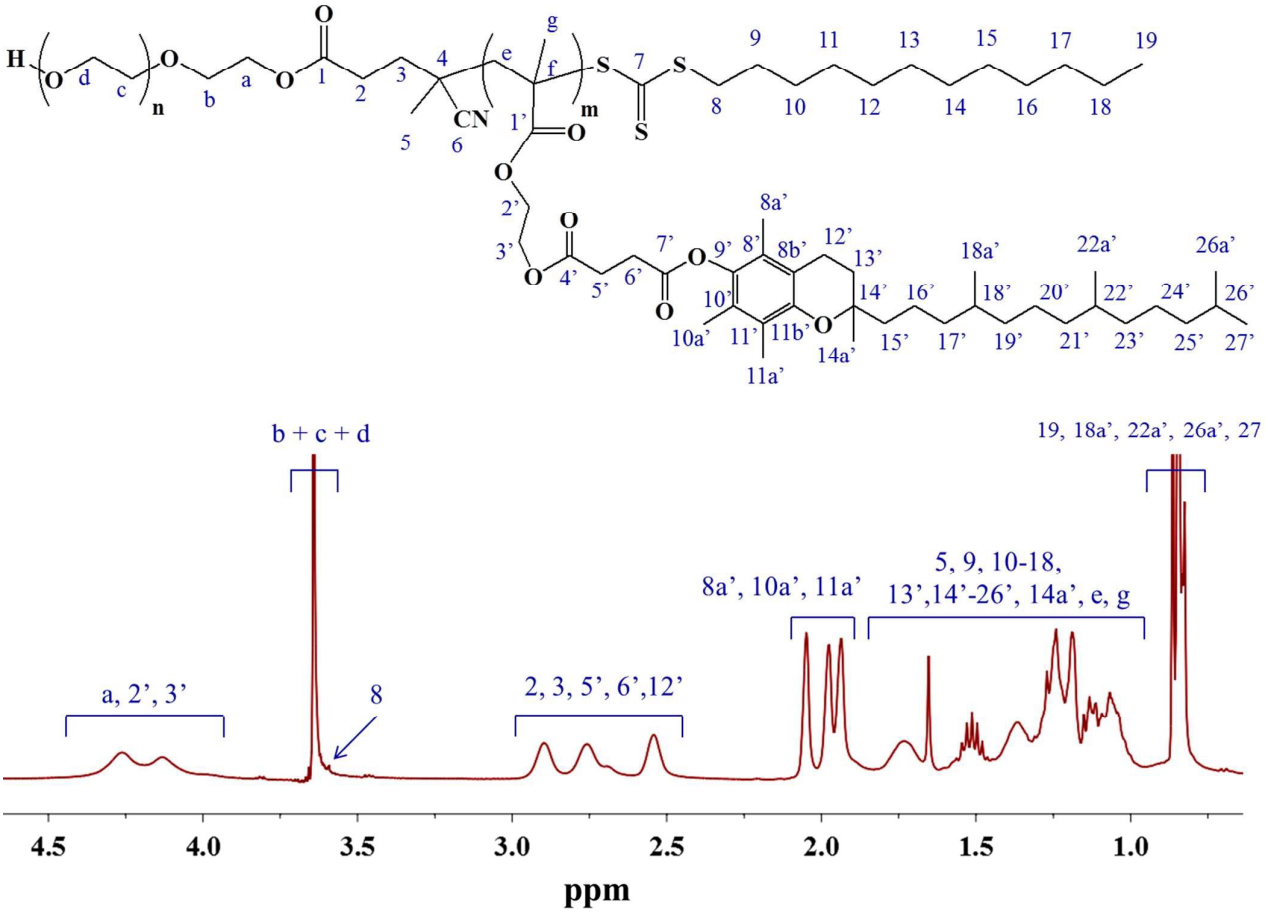

Figure 2: ^{1}H-NMR spectrum of PEG-71

Kinetics of RAFT polymerizations

The polymerization kinetics of MTOS with PEG macro-CTAs were investigated by analyzing the aliquots withdrawn from the polymerization mixture at different reaction times. Specifically, samples were analyzed by SEC and ^{1}H-NMR spectroscopy in order to quantify the MW and the Đ and to determine MTOS monomer conversion, respectively. Specifically, the conversion of MTOS was calculated by considering the vinyl proton signal at 6.1 ppm that disappeared over reaction time and the signal at 0.8 ppm corresponding to 12 protons of MTOS, that did not change during the polymerization reaction (**figure S4**, see Supporting Information).

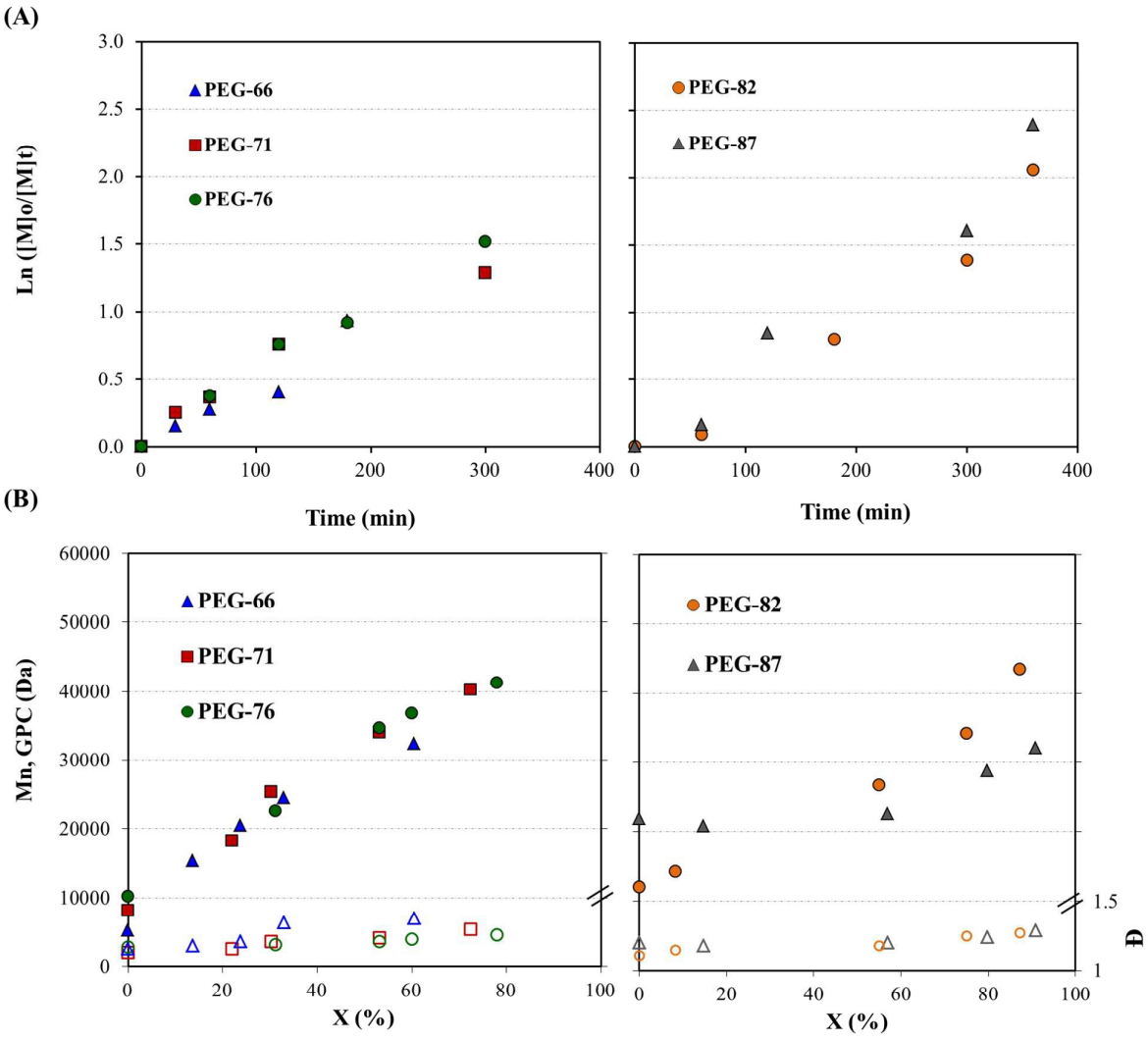

Figure 3: Kinetics of polymerization of PEG-*b*-poly(MTOS) copolymers. (A) $Ln([M]_o/[M]_t)$ plotted against reaction time and (B) M_n and Đ values as a function of MTOS conversion for PEG-66 (Blue), PEG-71 (Red), PEG-76 (Green), PEG-82 (Orange) and PEG-87 (Grey) amphiphilic block copolymers.

Figure 3 shows the polymerization kinetics of all synthesized block copolymers. In all cases, the evolution of $Ln([M]_0/[M]_t)$ as the function of time revealed a linear first order kinetic dependence, indicating a constant free radical concentration and, thus, the absence of significant terminations reactions. Additionally, the linear increase of M_n with conversion demonstrated the appropriate control over the polymerization of MTOS[12].

In the case of the MTOS polymerization with CTA-$PEG_{5\text{-}10}$, the ratio [MTOS]:[CTA]:[AIBN] was maintained constant and, therefore, the concentration of radicals was not varied. Polymerization rates did not correlate with the PEG MW and depended on the concentration of free radicals as expected.

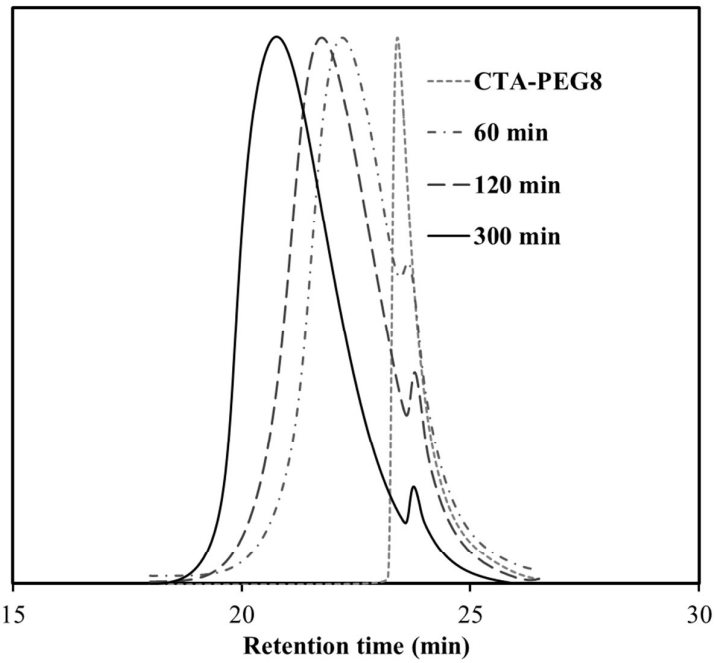

Figure 4: SEC traces as a function of a time polymerization of MTOS using CTA-PEG_8

The monomer concentration (M) was reduced when using macro-CTA agents with the highest MW of PEG (CTA-PEG_{12-22}). The polymerization should not be affected by changing this monomer concentration. However, the polymerization volume significantly increased and thus, the radical concentration decreased, leading to a reduction in polymerization rate. For that reason, the ratio [MTOS]:[CTA]:[AIBN] was changed, increasing the concentration of AIBN. This modification enhanced the polymerization rate in spite of the reduction of monomer concentration, avoiding the gelation of reaction product.

An example of the evolution of SEC traces during the RAFT polymerization is included in the **figure 4**. The traces were clearly shifted at lower elution times in comparison to the PEG macro-CTA agent as a function of the progression of the MTOS polymerization. Additionally, the SEC curves were bimodal indicating the presence of a minor fraction of unreacted PEG macro-CTA. This behavior is commonly observed for this type of polymerizations, indicating that the efficiency of macro CTA agents was not complete[53, 54]. Finally, it is noteworthy that no high MW species were observed at low retention times, confirming the absence of chain coupling reactions and the appropriate control over the RAFT polymerization. The molecular weight distributions were narrow as demonstrated by the relatively low dispersity (Đ <1.35).

Characterization of block copolymers

Block copolymers were exhaustively characterized after their purification by dialysis, that effectively eliminated the unreacted MTOS as a result of the non-full conversion reached and the mayority of low MW chains of the unreacted PEG macro-CTA agents. **Table 1** summarizes the most relevant characteristics of the prepared copolymers.

The composition of the different block copolymers was calculated based ^{1}H-NMR spectroscopy, using the integrals of the signals between 3.55-3.75 ppm assigned to 4 protons of PEG (CH-e', CH_2-4''') and the signal between 1.84 and 2.2 ppm (CH_3-8a', CH_3-10a', CH_3-11a') corresponding to 9 protons of MTOS (**figure S4**, see Supporting Information).

Table 1: Summary of most relevant structural characteristics of PEG-*b*-poly(MTOS) amphiphilic copolymers.

Sample	CTA-PEG	[a] M_n x 10^{-3}	[b] $M_{n\ theo}$ x 10^{-3}	[c] $M_{n\ SEC}$ x 10^{-3}	[c] Đ	[a] n_{PEG}	[a] m_{MTOS}	F_{PEG}-F_{MTOS} (mol %)	[d] T_{max} (°C)
PEG-66	CTA-PEG_5	42.9	44.4	38.8	1.35	111	58	66-34	381
PEG-71	CTA-PEG_8	54.3	54.4	48.4	1.27	177	73	71-29	394
PEG-76	CTA-PEG_{10}	55.6	60.3	51.8	1.23	223	71	76-24	392
PEG-82	CTA-PEG_{12}	59.5	67.9	50.5	1.27	266	56	82-18	404
PEG-87	CTA-PEG_{22}	68.5	80.2	37.7	1.29	487	73	87-13	403

a) Determinated using ^{1}H-NMR spectroscopy

b) Calculated applying the equation $Mn_{theo} = ([MTOS]/[CTA]*X_{MTOS}*100*MW_{MTOS}) + MW_{CTA}$

c) Determinated by SEC (THF) using PMMA standards

d) Measured by TGA under nitrogen atmosphere

The MTOS molar composition significantly decreased with increasing of the PEG MW, varying between 13 and 34 %-mol. This variable will be crucial to explain the amphiphilic properties of polymeric systems and their capacity to self-assembly in aqueous media, as will be described in the following sections. Additionally, the MW of block copolymers (calculated based on ^{1}H-NMR spectroscopy) was slightly lower in comparison to the theoretical value, being more pronounced with the increment of PEG MW of the macro CTA agents. This difference can be explained based on the reduction

of the efficiency of macro RAFT agents as a function of PEG MW. In fact, the SEC traces of different copolymerization reactions before their purification revealed that the narrow peak at a high retention time, associated to the PEG macro-CTA, significantly increased with the number of PEG units in the macro RAFT agents (see **figure S5**, Supplementary data). In the case of PEG-82, this peak overlaps with the peak of the block copolymer due to its high molecular weight. After the purification of block copolymers, unreacted PEG macro-CTA concentrations are very low and their incorporation in the self-assembling process of amphiphilic macromolecules will be not favored.

Results of M_n and Đ calculated by SEC are also shown in the **table 1**. It is noteworthy that these values were significantly lower than those obtained theoretically or by ^{1}H NMR spectroscopy. In this case, this deviation is most likely due to the PMMA calibration curve that was used to quantify the SEC measurements. Furthermore, Đ values were lower than 1.35, confirming the good control of the polymerization, obtaining well-defined amphiphilic block copolymers.

The thermal stabilities of block copolymers were investigated by TGA under nitrogen atmosphere. The TGA curves of different block copolymers are compared in the **figure S6** (see Supporting Information). Weight-loss rate of all block copolymers presented a maximum between 380 and 403 ºC that increased with the content of PEG in the copolymers. Moreover, these values were lower in comparison to the maximum degradation temperatures of PEG macro RAFT agents due to the incorporation of MTOS. In fact, TGA curves presented a shoulder at the temperature range from 300-350 ^{o}C that significantly increased with the MTOS content.

Characterization of self-assembled NPs

Amphiphilic block copolymers are excellent candidates for the preparation of micellar drug nanocarriers. Particularly, PEG-*b*-poly(MTOS) family presented a precise architecture with two well-defined hydrophilic and hydrophobic blocks. The appropriate hydrophilic/hydrophobic balance of these macromolecules will give rise to the self-organization of these polymer chains in aqueous media[7, 55, 56]. In the following sections, self-assembled NPs will be appointed as a function of the PEG molar composition in the polymeric systems. As an example, NPs prepared from PEG-71 will be labelled as NP-71.

Surfactant-free NPs were prepared by SORP or solvent exchange. This procedure has advantages in comparison to other alternatives, such as the conventional nanoprecipitation. SORP can be used to a wide type of polymeric materials, such as block copolymers, in order to obtain particles from nanometers to a micrometer scale. This simple methodology allows the progressive organization of amphiphilic chains due to the slow addition of aqueous phase drop to drop, avoiding the use of surfactants or protective colloids[40, 57, 58].

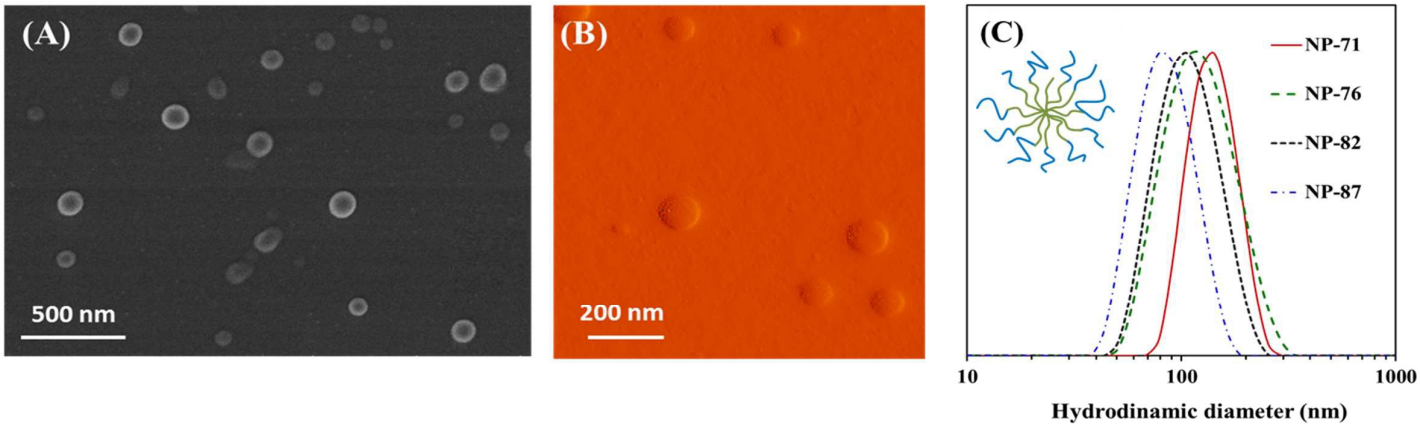

Figure 5: SEM (A) and AFM (B) micrographs of NP-71 polymeric systems dried from aqueous solution at room temperature. (C) Particle size distributions (D_h, by intensity) of unloaded NP, measured by DLS. Red: NP-71; Green: NP-76; Black: NP-82; Blue: NP-87.

The morphology of self-assembled NPs was confirmed by SEM and AFM. Representative micrographs of NP-71 are shown in the **figure 5**. These images confirmed the spherical morphology of NPs. The amphiphilic NPs had typical core-shell morphology with a MTOS hydrophobic core that was stabilized by a hydrophilic shell based on PEG chains.

Results of the most relevant characteristic of unloaded NPs are summarized in **table 2**. The preparation of stable NPs could not be achieved using the PEG-66 polymeric system, due to an unsuitable hydrophobic/ hyprophilic balance.

Table 2. Most relevant characteristics of unloaded and c6 NPs: Hydrodynamic diameter (D_h, by intensity), size distribution width (W_d), polydispersity index (PDI); and zeta potential values (ζ), measured by DLS and LDE respectively.

NP Sample	EE (%)	D_h (nm)	W*d* (nm)	PDI	ζ (mV)
NP-71	---	134.9 ± 6.5	31	0.079 ± 0.012	-2.38
NP-76	---	110.2 ± 4.3	47	0.101 ± 0.014	-1.08
NP-82	---	100.8 ± 5.8	31	0.087 ± 0.011	-0.68
NP-87	---	87.9 ± 2.6	27	0.079 ± 0.009	-0.16
NP-71 + c6	92.4	159.8 ± 8.8	43	0.079 ± 0.009	-0.68
NP-76 + c6	91.2	156.8 ± 3.3	55	0.056 ± 0.008	-0.60
NP-82 + c6	91.0	133.7 ± 4.4	62	0.044 ± 0.013	-0.51
NP-87 + c6	90.3	90.2 ± 5.7	49	0.080 ± 0.010	-0.44

In the other copolymeric systems, particle size varied between 88 and 135 nm with optimal values of PDI, below 0.1. Additionally, particle size distributions were narrow and unimodal with a width less than 50 nm for all compositions (**figure 5 C**). These results confirmed that the controlled polymerization of MTOS with an PEG-based hydrophilic block favoured the self-assembly of the macromolecular chains in aqueous media, obtaining defined NP sizes that are suitable for their application in cancer treatments, improving their endocytosis and accumulation in tumor tissues by the Enhanced Permeability and Retention Effect (EPR)[59, 60].

It is noteworthy that the hydrodynamic diameter of NPs decreased with increasing of PEG content in the copolymeric systems. This trend could be explained due to the presence of PEG in the external shell of NP that could stabilize them through inter- and intramolecular interactions[61, 62]. In fact, it is well-known that PEG can also form hydrogen bonds with the aqueous environment and its presence has also multiple advantages such as the effectively protection of NPs against hydrolysis or enzymatic degradation and the prevention of their recognition by RES[63, 64].

Additionally, the characteristic of NPs can be regulated as a function of the chemical composition, MW and the block lengths of the amphiphilic copolymers. In this sense, their synthesis by RAFT polymerization facilitates the easy and controlled modification of these different variables. These changes would not be possible if other polymerization techniques had been used, such as conventional radical polymerization. Recently, our group described the preparation of amphiphilic NPs based on MTOS that were copolymerized with VP by free radical polymerization (poly(VP-*co*-MTOS))[38]. In this case, control over the microstructure was only possible due to the different reactivity of the amphiphilic monomers. As a result, nanoparticles presented PDI values

higher than 0.1 and higher distribution width in comparison to these block copolymers[38].

The organization of amphiphilic macromolecular chains into nano-assemblies affected the properties of the copolymeric systems. As an example, an interesting comparison of the thermal degradation of PEG-71 and PEG-76 and their corresponding NPs is illustrated in the **figure 6**. The normalized curves of the derivative weight loss of both NP systems showed three defined peaks in comparison to the polymeric systems. On the one hand, the degradation peaks corresponding to MTOS and PEG were more defined in the NP systems. On the other hand, a new degradation peak appeared at an intermediate temperature. This new degradation stage could be due to the interface of these NPs with a core-shell morphology, the formation of inter- and intramolecular interactions that facilitated the stabilization of surfactant-free NP and finally the segregation of PEG and MTOS based domains

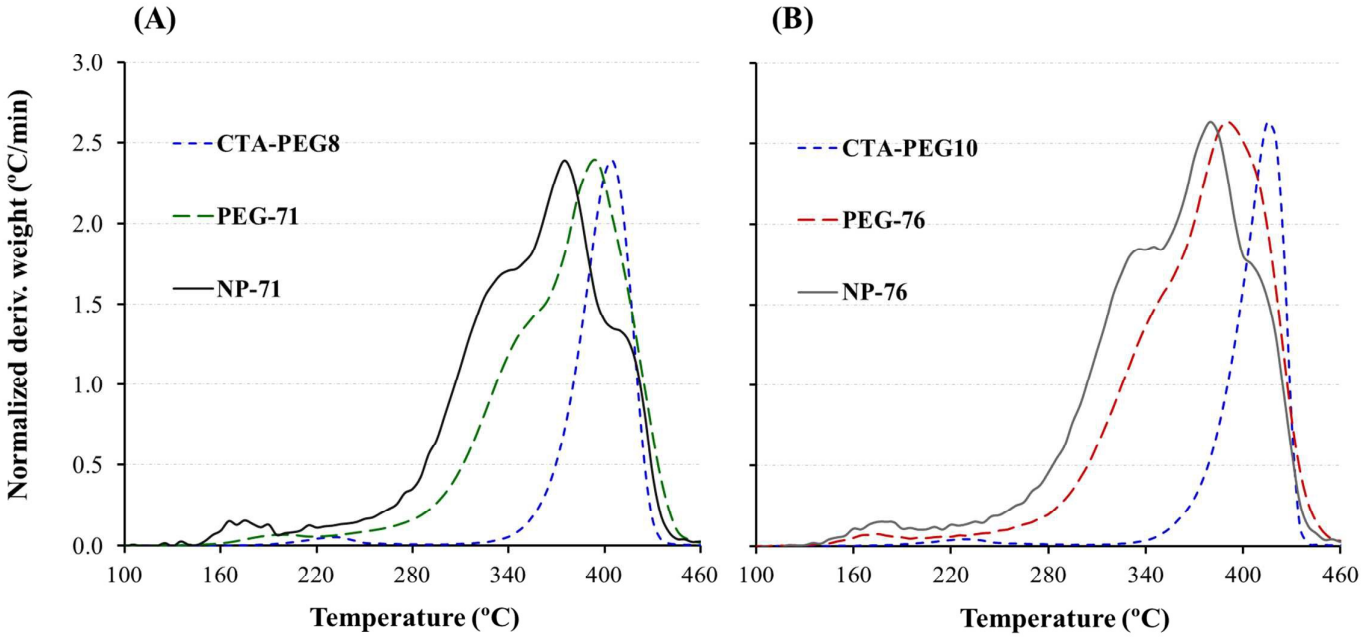

Figure 6: Overlay of normalized curves of derivative weight loss of (A) PEG-71 and (B) PEG-76 polymeric systems and their corresponding self-assembled NPs.

Finally, all NPs had a nearly neutral charge on their surface, exhibiting slightly negative zeta potential values similar to the zeta potential values in the same magnitude order described for other PEG nano-assemblies[65]. Such neutral charge of PEG-based nanoparticles is based on the absence of the charged groups in its structure. Additionally, the neutral charge of NP slightly increased with the increasing of PEG number units into the NP surface.

Coumarin-6 monitorization

The first step towards examining the therapeutic action of self-assembled NPs is characterizing the ability of polymeric systems to cross the cellular membrane of cancer cells in order to exert their biological activity. In this way, c6 was efficiently encapsulated in the core of the NPs (EE higher than 90%) and, thus, was used as a fluorescent probe to trace the NP within cancer cells.

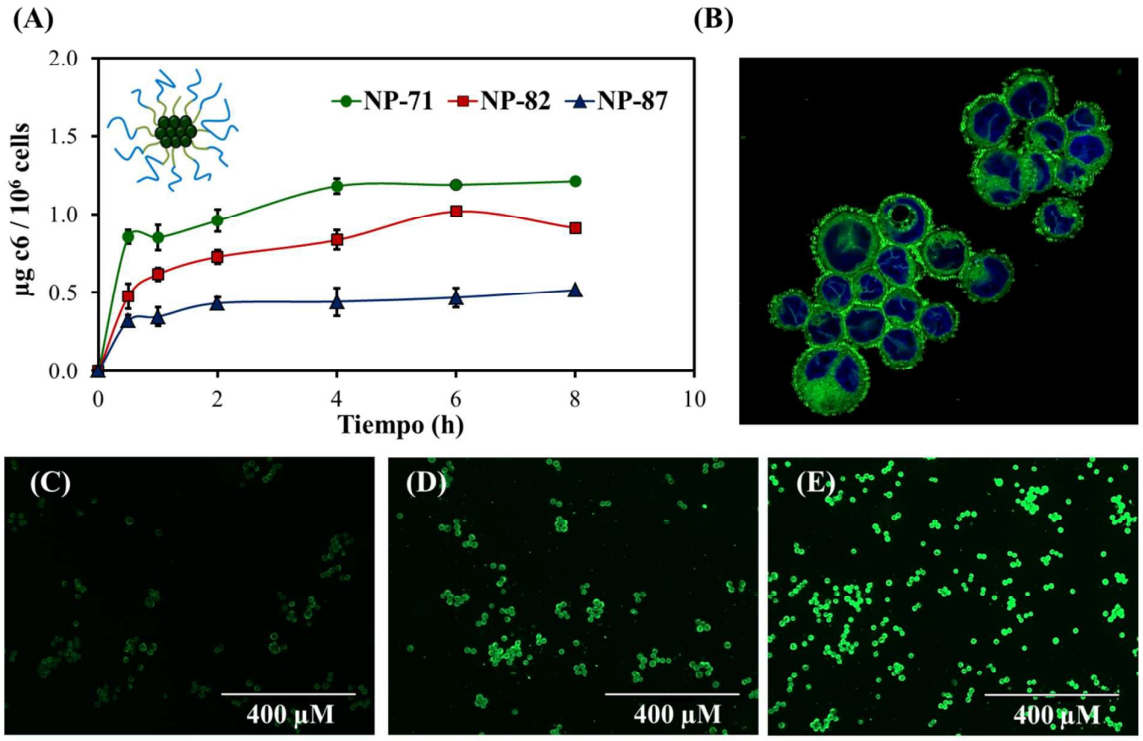

Figure 7: (A) Accumulated uptake of c6 loaded NPs in MDA-MB-453 cells along 8 h after the NPs incubation. Green: NP-71; Red:NP-82 and Blue: NP-87 (B) Confocal micrographs of MDA-MB-453 cells after 5 hours in contact with c6-NP-71. Fluorescent micrographs of MDA-MB-453 cells in 2D culture after 30 min (C), 4 (D) and 8 hours (E) in contact with c6-NP-71.

The green fluorescence of c6 entrapped NPs was quantified in a MDA-MB-453 cell culture along 8 h after the NP incubation, also studying the effect to vary the PEG length into the polymeric NPs. As shown in **figure 7**, the accumulation of c6 in MDA cells was gradually enhanced over time in all cases. This effect can be appreciated in the increment of fluorescence of the micrographs of cancer cells that were obtained after 30 min, 4 and 8 h in contact with c6-NP-71 using the fluorescence microscopy. Additionally, these fluorescence results demonstrated that the cellular uptake was significantly diminished as a function of PEG composition into the NPs. In fact, the longer the PEG segment the slower the cellular uptake of NPs. This phenomenon is known in the literature as the "PEG dilemma" that significantly decreases the interaction between polymeric NPs and the cell surface membrane and therefore, their therapeutic action, as will be demonstrated in the next section[66, 67].

After 5 h, c6-NP-71 were observed under the confocal microscopy revealing that self-assembled nanoparticles were located inside the cytoplasm of cancer cells around the nucleous, probably by an endocytosis mechanism[68]. Specifically, confocal micrographs (**figure 7 B**) allowed to observe that the cellular membrane of MDA cells was clearly affected as a result of NP treatment.

Anticancer activity

Human epidermal growth factor receptor 2 (HER2) overexpressing breast tumors constitute an aggressive disease subtype that results in poor prognosis[69-71]. HER2 has therefore emerged as a viable molecular target for disease treatment[72, 73]. Resistances to HER2-targeted therapies such as Trastuzumab that have emerged in the recent years[74], however, warrants the development of alternative therapeutic strategies to treat HER2-positive breast cancer.

In vitro biological activity of block copolymer NPs was therefore evaluated against HER2 positive human adenocarcinoma MDA-MB-453 cells. Cell viability was assessed using Alamar Blue. **Figure 8** shows the MDA-MB-453 cell viability after the treatment with different concentrations (between 2.50 and 0.16 mg/mL) of the NPs for 24 h.

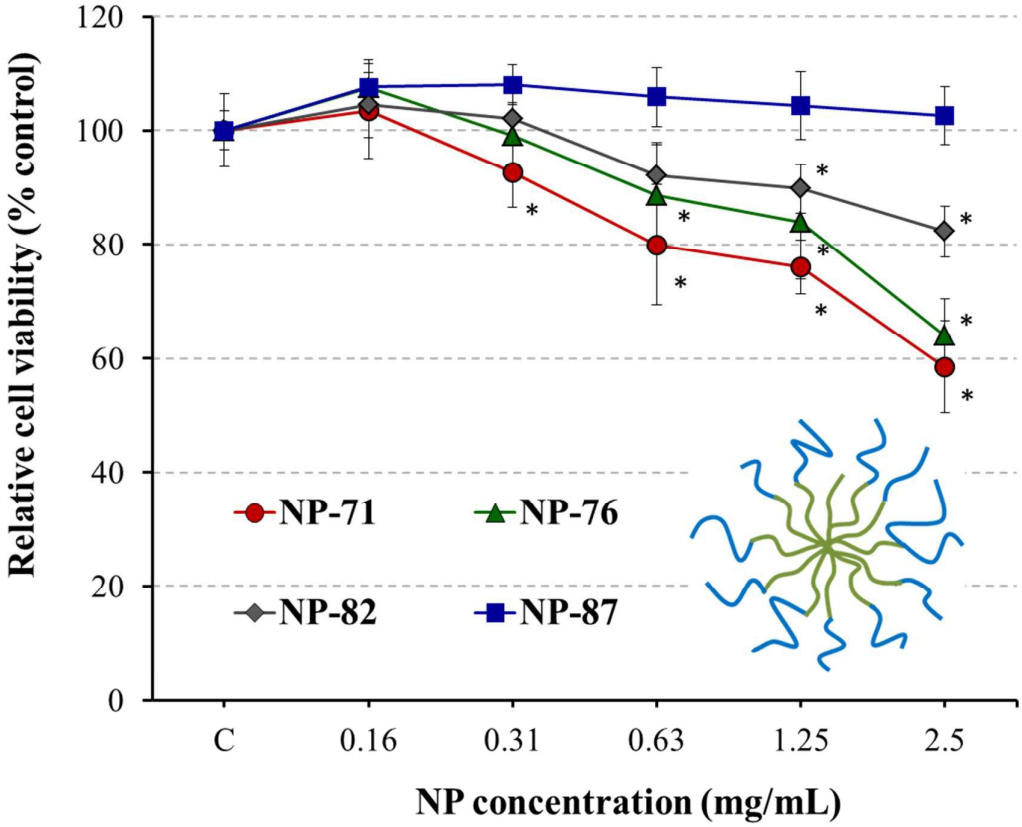

Figure 8: MDA-MB-453 viability in the presence of different NP concentrations, measured after 24 h with respect to the control. The diagrams include the mean, the standard deviation (n=8), and the ANOVA results at a significance level of *: $p < 0.05$.

In fact, cell viability decreased in a dose-dependent manner as a function of the NP concentration. Particularly, cell viability was reduced to around 60% in those formulations with the highest MTOS content (NP-71 and NP-76 with 29 and 24 mol- % of MTOS in the block copolymer, respectively) at 2.5 mg/mL. This cytotoxicity was only maintained at this highest NP concentration. Therefore, NP-71 and NP-76 formulations demonstrated anticancer activity in spite of the esterification of terminal carboxylic group of α-TOS that was performed in order to obtain a polymerizable methacrylic monomer. Neuzil et al. previously examined the mechanism of action of this mitocan and found its succinate group to be the functional domain that resulted in cell apoptosis due to increases in ROS within the mitochondria of exposed cells[16].

In contrast, NP-82 and NP-87 formulations were not cytotoxic with viabilities higher than 80% for all NP concentrations, in spite of their lower particle size if compared with NP-71 and NP-76. Our group recently described the anticancer activity of MTOS-based NP based on poly(VP-*co*-MTOS) pseudo-block copolymer[38]. The most active NP from this family of copolymer only presented 11 mol% of MTOS in its structure and therefore it was remarkable that PEG-b-PMTOS copolymers with higher content on MTOS were less active[38].

As it was previously mentioned, PEG was selected as hydrophilic block due to its well-known stealth properties that increase the circulation time in blood and its ability to minimize opsonization and resulting immune response. MW, surface chain density and conformation of PEG macromolecules are critical parameters to regulate their stealth

properties. Particularly, MW higher than 2000 are desired to guaranty the flexibility of PEG chains. The surface density directly affects the configuration of PEG chains and their mobility. At a high surface coverage, PEG chains have a brush configuration that completely covers the surface of NP and in contrast, reduces their mobility. The PEG chains adopt a mushroom configuration at a low surface coverage that can facilitate the presence of gaps where opsonins can bind to the surface[33].

On the other hand, the incorporation of too much PEG prevented cellular uptake by endocytosis due to the PEG dilemma.. In this sense, the loss of anticancer activity of synthesized NP with high PEG MW (NP-82 and NP-87 formulations) not only depended on the MTOS content, but also the PEG segment length. These results suggest the importance of an appropriate balance between the escape from the RES system and the control cellular uptake of PEGylated NPs, adjusting the MW of PEG chain and the hydrophobic and hydrophilic balance of macromolecular chains into the NPs.

CONCLUSIONS

RAFT polymerization was used for the synthesis of amphiphilic block copolymers with controlled molecular weight and relatively low dispersity (Đ <1.35) using PEG macro-CTAs of different molecular weights to control the radical polymerization of MTOS. Block copolymers PEG-*b*-poly(MTOS) were obtained after the controlled polymerization of MTOS with appropriate hydrophobic/hydrophilic balances to self-assemble in aqueous media by SORP. Bioactive nanoparticles with unimodal size distributions and sizes between 88 and 135 nm were obtained. These nanoparticles were stable and were endocytosed by cancer cells as demonstrated by the experiments carried out with coumarin-6-loaded NPs. Biological experiments revealed that the anticancer activity of self-assembled NPs significantly enhanced with an increase in MTOS content in the macromolecular chains and the reduction of PEG MW that inhibited the endocytosis of nano-assemblies. Finally, these NPs could encapsulate and deliver hydrophobic drug enabling combined therapy. When decorated with targeting moieties, these therapeutic NP formulations have the potential to exhibit superior cytotoxicity and selective activity in eliminating cancer cells.

AUTHOR INFORMATION

Corresponding Author

*Telephone: +34 91 561 88 06; Fax: +34 91 564 48 53; Email: mraguilar@ictp.csic.es

Author Contributions

The manuscript was written through contributions of all authors. All authors have given approval to the final version of the manuscript.

Funding Sources

This work was funded by the Spanish Ministry of Economy and Competitiveness (MAT2010-18155) and CIBER BBN-ECO Foundation project.

ACKNOWLEDGMENTS

Authors would like to thank financial support from the Spanish Ministry of Economy and Competitiveness (MAT2010-18155), CIBER BBN-ECO Foundation project, and the National Institutes of Health Cell and Tissue Engineering Training Grant T32 GM008433. Authors also acknowledge, David Gómez, and Rosa Ana Ramírez and Mar Fernández for their help in SEM, and cell culture experiments, respectively. Samarendra Maji gratefully acknowledges FWO for the Pegasus Marie Curie Fellowship.

FIGURE CAPTIONS

Figure 1: Chemical structure of PEG-*b*-poly(MTOS). Scheme of the self-assembled NPs formation based on these block copolymers, prepared by SORP.

Figure 2: ^{1}H-NMR spectrum of PEG-71.

Figure 3: Kinetics of polymerization of PEG-*b*-poly(MTOS) copolymers. (A) Ln($[M]_o/[M]_t$) plotted against reaction time and (B) M_n and Đ values as a function of MTOS conversion for PEG,66 (Blue), PEG-71 (Red), PEG-76 (Green), PEG-82 (Orange) and PEG-87 (Grey) amphiphilic block copolymers.

Figure 4: SEC traces as a function of a time polymerization of MTOS using CTA-PEG_8

Figure 5: SEM (A) and AFM (B) micrographs of NP-71 polymeric systems dried from aqueous solution at room temperature. (C) Particle size distributions (D_h, by intensity) of unloaded NP, measured by DLS. Red: NP-71; Green: NP-76; Black: NP-82; Blue: NP-87.

Figure 6: Overlay of normalized curves of derivative weight loss of (A) PEG-71 and (B) PEG-76 polymeric systems and their corresponding self-assembled NPs.

Figure 7: (A) Accumulated uptake of c6 loaded NPs in MDA-MB-453 cells along 8 h after the NPs incubation. Green: NP-71; Red: NP-82 and Blue: NP-87 (B) Confocal micrographs of MDA-MB-453 cells after 5 hours in contact with c6-NP-71. Fluorescent micrographs of MDA-MB-453 cells in 2D culture after 30 min (C), 4 (D) and 8 hours (E) in contact with c6-NP-71.

Figure 8: MDA-MB-453 viability in the presence of different NP concentrations, measured after 24 h with respect to the control. The diagrams include the mean, the standard deviation (n=8), and the ANOVA results at a significance level of *: $p < 0.05$.

TABLE CAPTIONS

Table 1: Summary of most relevant structural characteristics of PEG-*b*-poly(MTOS) amphiphilic copolymers.

Table 2. Most relevant characteristics of unloaded and c6 NPs: Hydrodynamic diameter (D_h, by intensity), size distribution width (W_d), polydispersity index (PDI); and zeta potential values (ζ), measured by DLS and LDE respectively.

REFERENCES

1. I. F. Uchegbu and A. Siew, *Journal of pharmaceutical sciences*, 2013, **102**, 305-310.
2. R. Wang, P. S. Billone and W. M. Mullett, *Journal of Nanomaterials*, 2013, **2013**, 1-12.
3. X. Xu, W. Ho, X. Zhang, N. Bertrand and O. Farokhzad, *Trends in molecular medicine*, 2015, **21**, 223-232.
4. L. Y. Rizzo, B. Theek, G. Storm, F. Kiessling and T. Lammers, *Current opinion in biotechnology*, 2013, **24**, 1159-1166.
5. J. H. Park, S. Lee, J.-H. Kim, K. Park, K. Kim and I. C. Kwon, *Progress in Polymer Science*, 2008, **33**, 113-137.
6. M. C. Branco and J. P. Schneider, *Acta biomaterialia*, 2009, **5**, 817-831.
7. A. Rösler, G. W. Vandermeulen and H.-A. Klok, *Advanced drug delivery reviews*, 2012, **64**, 270-279.
8. S. Parveen, R. Misra and S. K. Sahoo, *Nanomedicine: Nanotechnology, Biology and Medicine*, 2012, **8**, 147-166.
9. U. Kedar, P. Phutane, S. Shidhaye and V. Kadam, *Nanomedicine: Nanotechnology, Biology and Medicine*, 2010, **6**, 714-729.
10. B. Louage, Q. Zhang, N. Vanparijs, L. Voorhaar, S. Vande Casteele, Y. Shi, W. E. Hennink, J. Van Bocxlaer, R. Hoogenboom and B. G. De Geest, *Biomacromolecules*, 2015, **16**, 336-350.
11. W. A. Braunecker and K. Matyjaszewski, *Progress in Polymer Science*, 2007, **32**, 93-146.
12. D. J. Keddie, *Chemical Society Reviews*, 2014, **43**, 496-505.
13. A. W. York, S. E. Kirkland and C. L. McCormick, *Advanced drug delivery reviews*, 2008, **60**, 1018-1036.
14. J. Neuzil, L.-F. Dong, J. Rohlena, J. Truksa and S. J. Ralph, *Mitochondrion*, 2013, **13**, 199-208.
15. J. Neuzil, T. Weber, N. Gellert and C. Weber, *British journal of cancer*, 2001, **84**, 87-89.
16. J. Neuzil, L.-F. Dong, L. Ramanathapuram, T. Hahn, M. Chladova, X.-F. Wang, R. Zobalova, L. Prochazka, M. Gold and R. Freeman, *Molecular aspects of medicine*, 2007, **28**, 607-645.
17. K. Kluckova, A. Bezawork-Geleta, J. Rohlena, L. Dong and J. Neuzil, *Biochimica et Biophysica Acta (BBA)-Bioenergetics*, 2013, **1827**, 552-564.
18. J. Neuzil, J. Cerny, J. C. Dyason, L. F. Dong and S. J. Ralph, *Molecular nutrition & food research*, 2011, **55**, 1543-1551.
19. J. Neuzil, J. C. Dyason, R. Freeman, L.-F. Dong, L. Prochazka, X.-F. Wang, I. Scheffler and S. J. Ralph, *Journal of bioenergetics and biomembranes*, 2007, **39**, 65-72.
20. N. Duhem, F. Danhier and V. Préat, *Journal of Controlled Release*, 2014, **182**, 33-44.
21. N. Duhem, F. Danhier, V. Pourcelle, J.-M. Schumers, O. Bertrand, C. c. S. LeDuff, S. Hoeppener, U. S. Schubert, J.-F. o. Gohy and J. Marchand-Brynaert, *Bioconjugate chemistry*, 2013, **25**, 72-81.

22. H. J. Youk, E. Lee, M. K. Choi, Y. J. Lee, J. H. Chung, S. H. Kim, C. H. Lee and S. J. Lim, *Journal of controlled release : official journal of the Controlled Release Society*, 2005, **107**, 43-52.
23. Z. Zhang, L. Mei and S.-S. Feng, *Nanomedicine*, 2012, **7**, 1645-1647.
24. E. Bernabeu and D. A. Chiappetta, *Journal of Biomaterials and Tissue Engineering*, 2013, **3**, 122-134.
25. Z. Zhang, S. H. Lee and S.-S. Feng, *Biomaterials*, 2007, **28**, 1889-1899.
26. H. Chen, Y. Zheng, G. Tian, Y. Tian, X. Zeng, G. Liu, K. Liu, L. Li, Z. Li and L. Mei, *Nanoscale Res Lett*, 2011, **6**, 1-10.
27. W. Tao, X. Zeng, T. Liu, Z. Wang, Q. Xiong, C. Ouyang, L. Huang and L. Mei, *Acta biomaterialia*, 2013, **9**, 8910-8920.
28. H. N. Nguyen, T. M. N. Hoang, T. T. T. Mai, T. Q. T. Nguyen, H. D. Do, T. H. Pham, T. L. Nguyen and P. T. Ha, *Advances in Natural Sciences: Nanoscience and Nanotechnology*, 2015, **6**, 1-8.
29. J. Pan and S.-S. Feng, *Biomaterials*, 2008, **29**, 2663-2672.
30. P.-Y. Li, P.-S. Lai, W.-C. Hung and W.-J. Syu, *Biomacromolecules*, 2010, **11**, 2576-2582.
31. E. Bernabeu, G. Helguera, M. J. Legaspi, L. Gonzalez, C. Hocht, C. Taira and D. A. Chiappetta, *Colloids and Surfaces B: Biointerfaces*, 2014, **113**, 43-50.
32. L. Jiang, X. Li, L. Liu and Q. Zhang, *Nanoscale research letters*, 2013, **8**, 1-11.
33. J. V. Jokerst, T. Lobovkina, R. N. Zare and S. S. Gambhir, *Nanomedicine*, 2011, **6**, 715-728.
34. P. Suárez, L. Rojo, Á. González-Gómez and J. S. Román, *Macromolecular bioscience*, 2013, **13**, 1174-1184.
35. L. García-Fernández, S. Halstenberg, R. E. Unger, M. R. Aguilar, C. J. Kirkpatrick and J. San Román, *Biomaterials*, 2010, **31**, 7863-7872.
36. F. Reyes-Ortega, G. Rodríguez, M. R. Aguilar, M. Lord, J. Whitelock, M. H. Stenzel and J. San Román, *Journal of Materials Chemistry B*, 2013, **1**, 850-860.
37. M. L. Donaire, J. Parra-Cáceres, B. Vázquez-Lasa, I. García-Álvarez, A. Fernández-Mayoralas, A. López-Bravo and J. San Román, *Biomaterials*, 2009, **30**, 1613-1626.
38. R. Palao-Suay, M. R. Aguilar, F. J. Parra-Ruiz, M. Fernández-Gutiérrez, J. Parra, C. Sánchez-Rodríguez, R. Sanz-Fernández, L. Rodrigáñez and J. S. Román, *Biomacromolecules*, 2015, **16**, 1566-1581.
39. H. Otsuka, Y. Nagasaki and K. Kataoka, *Advanced drug delivery reviews*, 2012, **64**, 246-255.
40. H. Yabu, *Bulletin of the Chemical Society of Japan*, 2012, **85**, 265-274.
41. B. Page, M. Page and C. Noel, *International journal of oncology*, 1993, **3**, 473-476.
42. Y. Chong, T. P. Le, G. Moad, E. Rizzardo and S. H. Thang, *Macromolecules*, 1999, **32**, 2071-2074.
43. D. J. Keddie, G. Moad, E. Rizzardo and S. H. Thang, *Macromolecules*, 2012, **45**, 5321-5342.
44. Y. Ikeda and Y. Nagasaki, in *Polymers in Nanomedicine,* ed. S. Kunugi and T. Yamaoka, Springer Berlin Heidelberg, 2012, PEGylation Technology in Nanomedicine, 115-140.
45. H. Otsuka, Y. Nagasaki and K. Kataoka, *Advanced Drug Delivery Reviews*, 2012, **64**, 246-255.
46. E. Velasquez, J. Rieger, F. Stoffelbach, B. Charleux, F. D'Agosto, M. Lansalot, P.-E. Dufils and J. Vinas, *Polymer*, 2013, **54**, 6547-6554.

47. J. Rieger, G. Osterwinter, C. Bui, F. o. Stoffelbach and B. Charleux, *Macromolecules*, 2009, **42**, 5518-5525.
48. N. Nakajima and Y. Ikada, *Bioconjugate chemistry*, 1995, **6**, 123-130.
49. C. A. G. N. Montalbetti and V. Falque, *Tetrahedron*, 2005, **61**, 10827-10852.
50. S.-Y. Han and Y.-A. Kim, *Tetrahedron*, 2004, **60**, 2447-2467.
51. F. M. Veronese and G. Pasut, *Drug Discovery Today*, 2005, **10**, 1451-1458.
52. A. Favier and M. T. Charreyre, *Macromolecular Rapid Communications*, 2006, **27**, 653-692.
53. M. Müllner, A. Schallon, A. Walther, R. Freitag and A. H. Müller, *Biomacromolecules*, 2009, **11**, 390-396.
54. S. Kumar, R. Acharya, U. Chatterji and P. De, *Langmuir*, 2013, **29**, 15375-15385.
55. Y. Mai and A. Eisenberg, *Chemical Society Reviews*, 2012, **41**, 5969-5985.
56. G. Gaucher, M.-H. Dufresne, V. P. Sant, N. Kang, D. Maysinger and J.-C. Leroux, *Journal of Controlled Release*, 2005, **109**, 169-188.
57. H. Yabu and S. Sato, *Colloid and Polymer Science*, 2013, **291**, 181-186.
58. H. Yabu, *Polymer journal*, 2013, **45**, 261-268.
59. H. Maeda, *Bioconjugate chemistry*, 2010, **21**, 797-802.
60. V. Torchilin, *Advanced drug delivery reviews*, 2011, **63**, 131-135.
61. D. Pozzi, V. Colapicchioni, G. Caracciolo, S. Piovesana, A. L. Capriotti, S. Palchetti, S. De Grossi, A. Riccioli, H. Amenitsch and A. Laganà, *Nanoscale*, 2014, **6**, 2782-2792.
62. G. Cai and H. Jiang, *Journal of Materials Science: Materials in Medicine*, 2009, **20**, 1315-1320.
63. H. Otsuka, Y. Nagasaki and K. Kataoka, *Advanced Drug Delivery Reviews*, 2012, **64,** Supplement, 246-255.
64. Y. Ikeda and Y. Nagasaki, *Journal of Applied Polymer Science*, 2014, **131**,1-10.
65. Y. Hu, J. Xie, Y. W. Tong and C.-H. Wang, *Journal of Controlled Release*, 2007, **118**, 7-17.
66. H. Hatakeyama, H. Akita and H. Harashima, *Advanced Drug Delivery Reviews*, 2011, **63**, 152-160.
67. H. Hatakeyama, H. Akita and H. Harashima, *Biological and Pharmaceutical Bulletin*, 2013, **36**, 892-899.
68. T.-G. Iversen, T. Skotland and K. Sandvig, *Nano Today*, 2011, **6**, 176-185.
69. M. A. Owens, B. C. Horten and M. M. Da Silva, *Clinical breast cancer*, 2004, **5**, 63-69.
70. S. Sjögren, M. Inganäs, A. Lindgren, L. Holmberg and J. Bergh, *Journal of Clinical Oncology*, 1998, **16**, 462-469.
71. D. J. Slamon, G. M. Clark, S. G. Wong, W. J. Levin, A. Ullrich and W. L. McGuire, *Science*, 1987, **235**, 177-182.
72. S. Vrbic, I. Pejcic, S. Filipovic, B. Kocic and M. Vrbic, *J buon*, 2013, **18**, 4-16.
73. D. L. Holliday and V. Speirs, *Breast Cancer Res*, 2011, **13**, 215.
74. G. Valabrega, F. Montemurro and M. Aglietta, *Annals of oncology*, 2007, **18**, 977-984.

GRAPHICAL ABSTRACT

RAFT block copolymers based on polyethylene glycol (PEG) and the methacrylic derivative of α-tocopheryl succinate (α-TOS) are synthesized and fully characterized. The well-defined architecture of the block copolymers gives rise to surfactant-free spherical nanoparticles by self-organized precipitation method. The *in vitro* biological activity of the NP is also explored.